Composite Structures 280 (2022) 114857

Contents lists available at ScienceDirect

Composite Structures

journal homepage: www.elsevier.com/locate/compstruct

Short communication

Active multi-physical modulation of Poisson's ratios in composite piezoelectric lattices: On-demand sign reversal

A. Singh [a,*,1], T. Mukhopadhyay [b,*,1], S. Adhikari [c,1], B. Bhattacharya [a,1]

[a] Department of Mechanical Engineering, Indian Institute of Technology Kanpur, Kanpur, India
[b] Department of Aerospace Engineering, Indian Institute of Technology Kanpur, Kanpur, India
[c] James Watt School of Engineering, University of Glasgow, Glasgow, United Kingdom

ARTICLE INFO

Keywords:
Active honeycomb lattices
Poisson's ratio modulation
On-demand sign reversal of elastic moduli
Multi-functional piezoelectric lattices

ABSTRACT

A large number of studies have been reported in literature to analyse various parameters that influence the Poisson's ratios of multi-functional lattice materials. However, the major limitation in such lattices is that once the lattice is manufactured, the Poisson's ratios and other elastic properties become fixed corresponding to the particular lattice configuration. This limits the application of such lattices in many advanced multi-functional structures and systems, where on-demand active property modulations are warranted. This paper proposes composite lattices comprising a substrate and piezoelectric materials, wherein it is possible to actively modulate the Poisson's ratios and other elastic properties as a function of voltage. Considering both axial and transverse deformations of the cell walls along with a unit cell based approach, the exact closed-form expressions of Poisson's ratios and equivalent Young's modulus are derived in an expanded design space for the unimorph and bimorph configurations. The study reveals that a sign reversal of the Poisson's ratios and Young's modulus can be achieved for specific combinations of cell angle and applied voltage. Contrary to the conventional wisdom, such active sign reversal implies that re-entrant honeycomb lattices can exhibit positive Poisson's ratios and vice versa.

1. Introduction

Two-dimensional lattice-based materials can be constructed by repeating the unit cell periodically. In general, microstructural geometry of the unit cells plays a vital role in determining the mechanical properties of the entire lattice. A large number of studies have been conducted considering various shapes of lattice structures such as hexagonal, square, Kagome, N- Kagome, triangular, star triangular honeycombs and other tailor-made geometries [1–8]. Such studies convincingly demonstrate that application-specific tailored unit cell geometries are capable of obtaining unprecedented mechanical behaviour of these artificially engineered materials (often referred as metamaterials) including multi-functional modulation of equivalent elastic moduli, vibration and wave propagation behaviour, negative Poisson's ratio, negative Young's modulus, direction-dependent stiffness, programmable shape modulation etc. [9–11]. In particular, Poisson's ratios of metamaterials have received significant attention from the scientific community due to its importance in far-field shape modulation and actuation applications along with other mechanical behaviour such as deformation, vibration, impact and indentation. Based on the intuitive design of microstructural lattice geometries, it is possible to achieve positive, negative and zero Poisson's ratios including extreme values [12–18]. However, the major limitation in such lattices is that once the lattice is manufactured, the Poisson's ratios and other elastic properties become fixed corresponding to the particular lattice configuration. This limits the application of such lattices in many advanced multi-functional structures and systems, where on-demand active property modulations are warranted. In this article, we embark on overcoming this lacuna with a focus on the Poisson's ratios by introducing active materials in the lattice configuration.

For planar 2D cellular materials, the closed-form analytical expressions (equivalent elastic moduli) have been presented extensively in literature due to their computational efficiency and rich physical insights [12,19–24]. The unusual negative values of longitudinal and transverse Young's modulus has been reported under dynamic conditions by Adhikari et al. [25] whereas, Singh et al. [26] discussed the occurrence of negative Young's modulus under static conditions. A general analytical approach to determine elastic properties considering

* Corresponding authors.
E-mail addresses: amangill@iitk.ac.in (A. Singh), tanmoy@iitk.ac.in (T. Mukhopadhyay), Sondipon.Adhikari@glasgow.ac.uk (S. Adhikari), bishakh@iitk.ac.in (B. Bhattacharya).
[1] All the authors have contributed equally to the research and subsequent preparation of the manuscript.

https://doi.org/10.1016/j.compstruct.2021.114857
Received 14 August 2021; Received in revised form 13 October 2021; Accepted 17 October 2021
Available online 10 November 2021

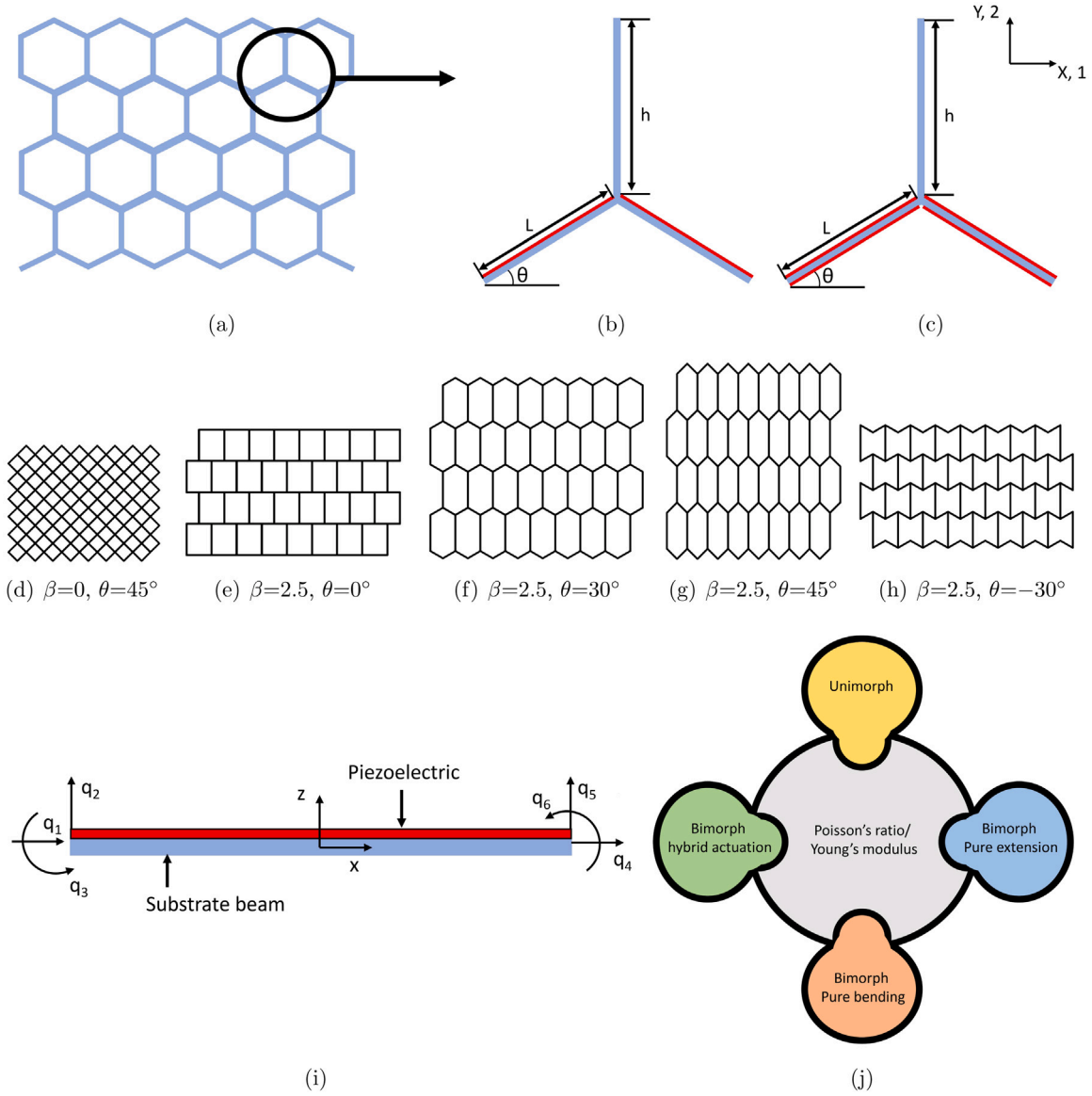

Fig. 1. Piezoelectric lattice microstructures for active multi-physical Poisson's ratio modulation. (a) Generic hexagonal honeycomb lattice microstructure representation in X–Y plane **(b)** Unimorph unit cell highlighting the length of vertical cell wall (h), inclined cell walls (L) and cell angle (θ). Note that the substrate beam is shown in blue colour, while the piezoelectric patches are indicated using red colour. **(c)** Bimorph unit cell highlighting the length of vertical cell wall (h), inclined cell walls (L) and cell angle (θ). Note that the substrate beam is shown in blue colour, while the piezoelectric patches are indicated using red colour. In the proposed microstructures, the piezoelectric patches are mounted over the inclined cell walls only. **(d)–(h)** Typical topologies of honeycomb lattices having different values of β (i.e., $\frac{h}{L}$ ratio) and cell angle (θ). Note that all these geometries can be readily analysed using the proposed analytical framework by considering corresponding geometric parameters. **(i)** Degrees of freedom for a single cell wall (i.e. hybrid beam) having a piezoelectric patch. A local coordinate system (x, z) has been taken to obtain the deformation of a single hybrid beam, where the direction x is along the beam length. Note that the effective displacement components of a unit cell under different loading and actuation conditions are obtained using the 6×6 stiffness matrix of a single beam element with the unimorph and bimorph configurations. The stiffness matrix of the vertical cell walls are same as that of a normal beam without any piezoelectric attachment. **(j)** A schematic representation of four different cases for which the Poisson's ratios and Young's moduli are analysed in the present study (refer to Fig. 2 for more details).

both axial and transverse displacements under dynamic condition has been studied by Adhikari et al. [27]. When only bending deformation of the cell walls are considered for a hexagonal honeycomb unit cell, it has been documented in the literature by Gibson and Ashby [19] that ν_{12} and ν_{21} are independent of material property and depend only on the microstructural geometry. Similar observation was reported in an earlier study of piezoelectric lattices [26], wherein only bending deformation of the cell walls was considered with the limitation of low thickness and high axial rigidity. Singh et al. [26] showed that while active voltage-dependent modulation of the in-plane Young's moduli is possible in such a hybrid hexagonal lattice, the Poisson's ratio's cannot be modulated as a function of voltage. In the current paper, we aim to include the effect of axial deformation of the cell walls in addition to the bending deformation, wherein it will be showed that the Poisson's ratios become functions of the applied voltage in addition to the microstructural geometry. This development will lead to on-demand active modulation of Poisson's ratios in piezoelectric lattice materials.

Most of the lattice structures exhibit positive Poisson's ratios, while there exist some lattice geometries that can exhibit negative Poisson's ratio [28,29]. Over the years, various forms of geometries (origami, chiral, star-shaped and foam structures) and structural mechanisms have been studied to obtain the negative Poisson's ratio [30–35]. It is well-established in the literature that Poisson's ratio for hexagonal honeycomb lattices is positive for positive cell angle (note that the parameter θ in Fig. 1(b, c) is referred as the cell angle) and vice

versa [36–38]. According to the general wisdom, it is not possible to have Positive Poisson's ratio in an auxetic (i.e. negative cell angle) configuration, or negative Poisson's ratio in a hexagonal lattice with positive cell angle. In this study, we would decouple this relation and extend the capability of active Poisson's ratio modulation to an extent where a sign reversal of Poisson's ratios is possible as a function of applied voltage.

As per the preceding discussions in this section, this paper aims to develop an active modulation capability of Poisson's ratios (including on-demand sign-reversal) in piezoelectric honeycomb lattices. Hybrid honeycomb lattice structures comprised of a substrate and piezoelectric material Dwivedi et al. [39],Crawley and Anderson [40],Crawley and de Luist [41] would be analysed considering both the unimorph and bimorph configurations (refer to Fig. 1). As an integral part of this study, the Young's moduli of such lattices would also be investigated. A bottom-up unit cell based analytical approach would be adopted to obtain the closed-form expressions of Poisson's ratios and the Young's moduli by taking into account both the axial and bending deformations of the cell walls. The Section 2 of this paper provides critical insights for the active modulation of Poisson's ratios and the Young's moduli including numerical illustrations. Note that the detailed derivations are provided in a separate supplementary document. The key highlights along with concluding remarks are presented in Section 3.

2. Active modulation of Poisson's ratios and other effective elastic properties

We demonstrate the concept of active Poisson's ratio modulation by considering hexagonal lattices and their derivatives, as depicted in Fig. 1. Such hexagonal lattices are made of substrate material (vertical cell walls) and a combination of substrate and piezoelectric material (inclined cell walls) as shown in Fig. 1(b–c). The unit cell comprises of three cell walls assumed to be Euler–Bernoulli beams connected to each other at specified cell angles, wherein a beam→unit cell→entire lattice bottom-up approach is followed to derive the closed-form analytical expressions for the Poisson's ratios and Young's moduli. To make the study more generic, both axial and bending deformations of the cell walls are considered [27]. Consideration of axial deformation, in turn, makes the Poisson's ratios voltage-dependent, leading to the capability of active modulation. The slant members contribute through bending and axial deformations while calculating both the in-plane Poisson's ratios. Note that the vertical members in the lattice structure can only contribute by means of axial deformation when the required deformation direction and direction of loading are parallel. The lattices being symmetric and periodic, there is no possibility of bending deformation for the vertical members, as the loading is either perpendicular or parallel to the axis of vertical members.

Note that the current tri-member unit cell has two types of beams; the vertical beam is a simple beam element without any piezo patches, while the slant beams are piezo embedded beams as described in Fig. 2. The static stiffness matrix of a normal beam element is widely reported in literature [27], while a detailed derivation of the voltage-dependent stiffness matrix for piezo-embedded beam configurations is provided in the supplementary material. The stiffness matrices are used in a unit cell-based framework to obtain the voltage-dependent elastic properties of the entire lattice. Here the in-plane elastic properties have been derived by subjecting the unit cell under the combined loading of externally applied mechanical stress and voltage. Hence, the strains in X and Y direction are obtained by calculating the transverse and axial displacements of the beam members of the unit cell, which can be categorized into two parts: displacement due to externally applied mechanical stress and displacement due to applied voltage (refer to the supplementary material for detailed derivation). In the present study, these displacements have been obtained in the form of stiffness matrix elements (K) in order to keep the formulation more general.

Table 1
Details of the parameters involved in the current analytical framework. Here K represents the 6 × 6 stiffness matrix of a generalized single hybrid beam (refer to the supplementary material) applicable to both unimorph and bimorph configurations. The subscripts refer to the element of the matrix following general conventions. The detailed derivation of the expressions for both unimorph and bimorph configurations has been provided in the supplementary material. Here, Y, W, T, V, V_t and V_b stands for Young's modulus, width, thickness, voltage, voltage in top and bottom piezoelectric material, respectively. In the subscript, s and p stands for the substrate and the piezoelectric material. Some non-dimensional ratios are defined in this work as, γ stands for substrate layer thickness to inclined cell wall length $\left(\frac{T_s}{L}\right)$, κ is piezoelectric to substrate material Young's modulus ratio $\left(\frac{Y_p}{Y_s}\right)$, α stands for piezoelectric to substrate beam thickness ratio $\left(\frac{T_p}{T_s}\right)$, β is the ratio of vertical cell wall length to inclined cell wall length $\left(\frac{h}{L}\right)$.

Parameter	Configuration	
	Unimorph	Bimorph
K_{44}	$Y_s W_s \gamma (1+\kappa\alpha)$	$Y_s W_s \gamma (1+2\kappa\alpha)$
K_{44}^h	$\frac{Y_s W_s \gamma (1+\kappa\alpha)}{\beta}$	$\frac{Y_s W_s \gamma (1+2\kappa\alpha)}{\beta}$
K_{55}	$Y_s W_s \gamma^3 \left(1+4\kappa\left(\alpha^3+1.5\alpha^2+0.75\alpha\right)\right)$	$Y_s W_s \gamma^3 \left(1+8\kappa\left(\alpha^3+1.5\alpha^2+0.75\alpha\right)\right)$
K_{64}	$-0.5 Y_p W_p \gamma T_s \alpha (1+\alpha)$	0
$B_p V$	$W_p d_{31} Y_p V$	$W_p d_{31} Y_p \left(V_t + V_b\right)$
$J_p V$	$0.5 W_p d_{31} Y_p T_s (1+\alpha) V$	$0.5 W_p d_{31} Y_p T_s (1+\alpha)\left(V_t - V_b\right)$

It is widely reported in the literature [12,19] that deformation behaviour influences the determination of the Poisson's ratio (ν_{12} and ν_{21}) and Young's modulus (E_1 and E_2). It has been studied by Singh et al. [26], that if only the bending deformation of the cell walls is considered or in other words cell walls are assumed to be axially rigid, then ν_{12} and ν_{21} come out to be independent of externally applied voltage and stress, making the active control of Poisson's ratios impossible. In this article, the inclusion of axial deformation to obtain the effective elastic moduli of honeycomb lattices has given rise to interesting insights concerning the Poisson's ratios. Due to the effect of axial deformation, it possible to modulate (voltage-dependent) Poisson's ratios (ν_{12} and ν_{21}) on-demand, along with the Young's modulus (E_1 and E_2). The proposed analytical framework in this article can be implemented for both tensile and compressive loading as well as for both polarities of voltage. We have discussed the voltage-dependent modulation of elastic moduli by considering different cases as shown in Fig. 1(j).

2.1. Poisson's ratio

As discussed in the preceding section, it is normally considered that the Poisson's ratios depend on the geometric properties of the periodic structure under investigation [12,19,26]. For positive cell angles (θ), Poisson's ratios are positive and vice-versa. In the current analysis of active piezoelectric lattices (including the physics of bending and axial deformation of the connecting beam-like members), the Poisson's ratios also depend on the externally applied stress and voltage along with geometric and material properties. In the subsequent numerical results, we also demonstrate that the coupling in the sign of cell angle and nature of Poisson's ratios can be broken in the current multi-physical regime. The derived analytical expressions for the Poisson's ratios ν_{12} and ν_{21} (refer to the supplementary material for detailed derivation) are presented in Eqs. (1) and (2). These expressions are independent of the unimorph and bimorph configuration (i.e. the closed-form expressions are presented in a general form). The parameters of these equations that would change with the unimorph and bimorph configurations have been mentioned in Table 1. Note here that B_p relates the voltage and extension coupling component, while J_p couples the voltage and curvature component. Here, K refers to the 6 × 6 stiffness matrix of a single-hybrid beam (inclined cell walls) and the subscripts of K refer to the element of the matrix.

$$\nu_{12} = \frac{\lambda_{P2}\cos^2\theta\,(\beta+\sin\theta) - \frac{B_p V \lambda_{BP2}}{\sigma_1 L W_s}\frac{K_{55}}{K_{44}} + \frac{6 J_p V \cos\theta \lambda_{JP2}}{\sigma_1 L^2 W_s}}{\lambda_{P1}\cos\theta\,(\beta+\sin\theta) + \frac{B_p V \lambda_{BP1}}{\sigma_1 L W_s}\frac{K_{55}}{K_{44}} + \frac{6 J_p V \lambda_{JP1}}{\sigma_1 L^2 W_s}} \tag{1}$$

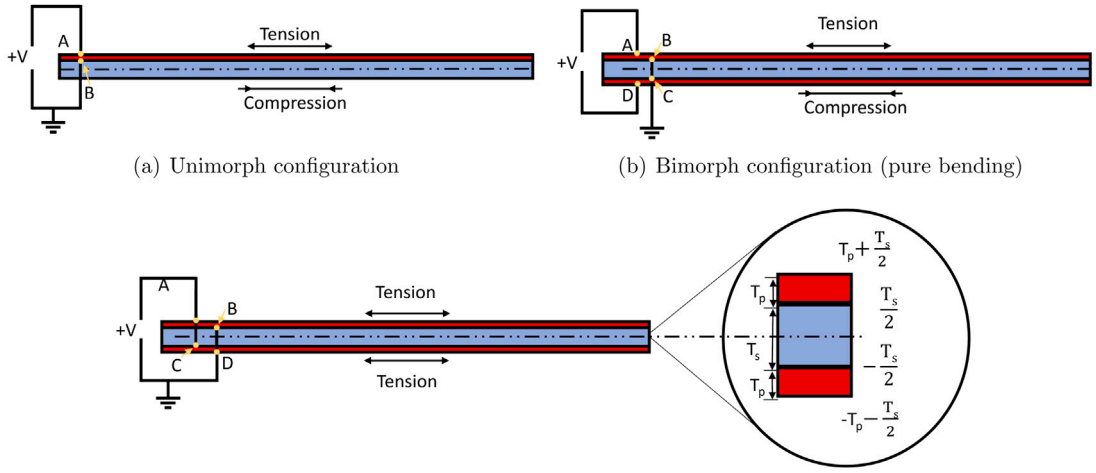

Fig. 2. Mechanics of element-level piezoelectric composite beams. Different beam configurations showing the intermediate limit points from the neutral axis (assumed to lie at the geometric centre of the substrate beam) are presented. Here we explain different possibilities of piezoelectric actuation as shown in Fig. 1(j). **(a)** Unimorph beam configuration and electrical connections. This configuration would result in pure bending. (b) Electrical connections required for pure bending under a bimorph configuration. Here both top and bottom piezoelectric materials are under the influence of opposite polarity, but the same magnitude of voltage, i.e., $V_t = -V_b$ (here, V_t and V_b stands for the voltage applied to the top and bottom piezoelectric layer, respectively). Under this type of voltage arrangement, only the curvature component (J_p) plays a role. (c) Electrical connections required for the pure extension to occur in bimorph configuration. Here both the top and bottom piezoelectric materials are under the influence of the same polarity and magnitude of voltage, i.e., $V_t = V_b$. Under this type of voltage, only the extensional component (B_p) plays a role. Note that one more scenario (hybrid actuation) is possible, wherein both top and bottom piezoelectric materials are influenced by different magnitude of voltage irrespective of the polarity. Both curvature and extensional components play a role in the deformation of such beams.

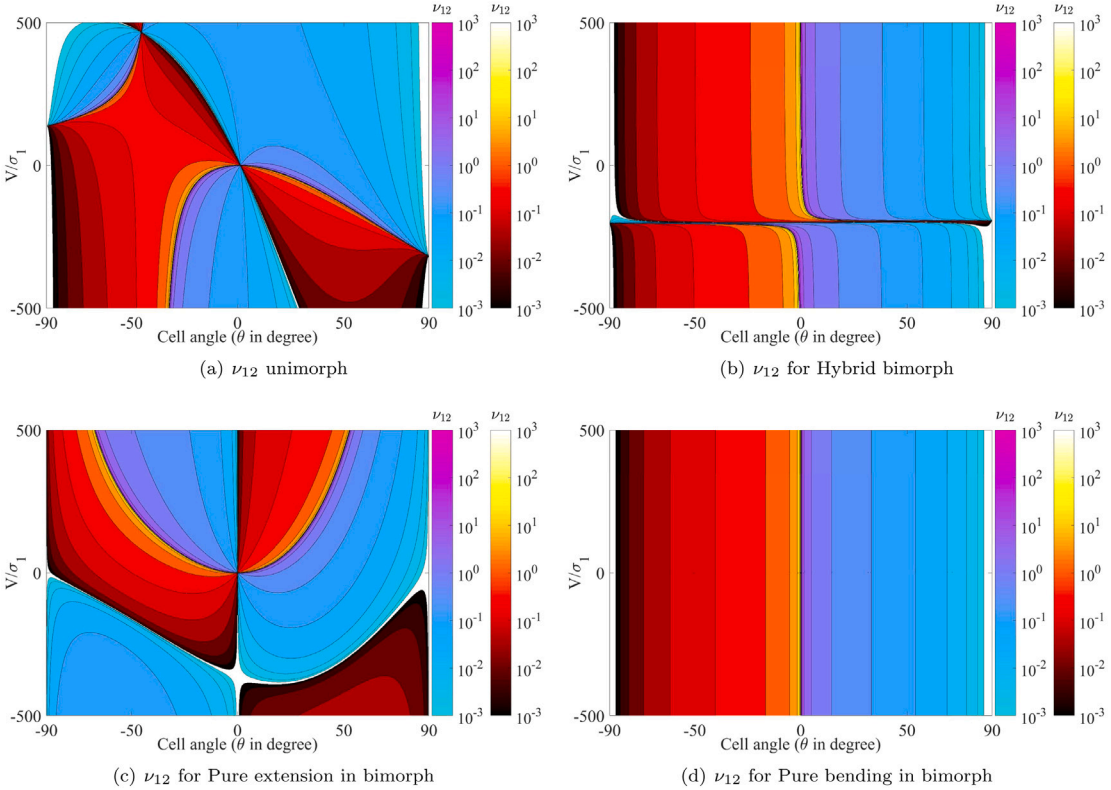

Fig. 3. Active modulation of ν_{12}. The Poisson's ratio ν_{12} has been plotted for all the different possible cases. (a) Unimorph configuration (b) Hybrid actuation in bimorph configuration (c) Pure extension in bimorph configuration (d) Pure bending in bimorph configuration. Variation in ν_{12} with cell angle and $\frac{V}{\sigma_1}$ (for hybrid bimorph $\frac{V_t}{\sigma_1}$ is varied and $\frac{V_b}{\sigma_1}$ has been kept equal to −200; V_t and V_b stand for the voltage applied to the top and bottom piezoelectric layer, respectively) ratio are analysed at a fixed value of $\beta = 2.5$. A clear reversal of sign for Poisson's ratio can be observed except for the case of pure bending and pure extension (bimorph). Note that the blue and red gradient in colour bar represents the positive and negative values.

$$\nu_{21} = \frac{\lambda_{W1}\cos^2\theta - \frac{B_p V \lambda_{BW1}}{\sigma_2 L W_s}\frac{K_{55}}{K_{44}} + \frac{6J_p V \lambda_{JW1}}{\sigma_2 L^2 W_s}}{\lambda_{W2}\cos^3\theta + \frac{B_p V \lambda_{BW2}}{\sigma_2 L W_s}\frac{K_{55}}{K_{44}} + \frac{6J_p V \cos\theta \lambda_{JW2}}{\sigma_2 L^2 W_s}} \tag{2}$$

The quantities λ_{P1}, λ_{P2}, λ_{BP1}, λ_{BP2}, λ_{JP1}, λ_{JP2}, λ_{W1}, λ_{W2}, λ_{BW1}, λ_{BW2}, λ_{JW1} and λ_{JW2} are functions of cell angle (θ), length of inclined cell wall (L) and elements of stiffness matrix [K] (refer to Appendix A for the closed-form expressions of these quantities). Note that the expressions of the matrix elements are different for unimorph and bimorph configurations as mentioned in Table 1 (refer to the supplementary material for detailed derivation). We have preferred to present the generic expressions of Poisson's ratios here as the parameters mentioned above help in making the formulation more general for unimorph and bimorph configurations through a unified framework. The subscripts of λ, P and W stand for load generated due to application of stress (σ) in direction 1 and 2 respectively, whereas B and J stand for the voltage to extensional component (B_p) and voltage to curvature component (J_p). The 1 and 2 in the subscript of λ states the strains in directions 1 and 2 respectively. The non-dimensional ratios defined in the formulation are given as $\gamma = \frac{T_s}{L}$, $\beta = \frac{h}{L}$, $\kappa = \frac{Y_p}{Y_s}$ and $\alpha = \frac{T_p}{T_s}$. It can be observed from Eq. (1) and Eq. (2) that ν_{12} and ν_{21} depend on voltage (V), material parameters (Y_p, Y_s, d_{31}), externally applied stress (σ_1, σ_2) and geometric parameters (θ, h, L, T_s, T_p).

The elastic properties (Poisson's ratios and Young's moduli, as presented in Eqs. (1), (2), (7) and (8)) of the unit cell and the entire lattice structure depend on the beam-level deformation mechanics under the multi-physical stress conditions. A beam-level numerical validation of the hybrid piezoelectric beams is provided in the supplementary material (refer to Section 1.2). Moreover, the proposed 3D lattice has been modelled in conventional finite element software COMSOL for further lattice-level validation (refer to Section 2.4 of the supplementary material). The comparison between the results obtained from the present formulation (using Eq. (1), (2), (7) and (8)) and the finite element based numerical simulation has been presented in Fig. 7 of the supplementary material. It can be observed that both the results lie in close proximity, providing the necessary credence for the developed analytical framework.

It is worthy to mention here that on substituting $V = 0$ and $\alpha = 0$ in the general expressions of Poisson's ratios and Young's moduli (i.e. Eq. (1), (2), (7) and (8)), we obtain the same expressions as given by Adhikari et al. [27] for passive lattices (refer to the supplementary material for further details), where the elastic moduli depend on the geometry of the unit cell and intrinsic material properties of the cell walls only. Note that the formulation of Adhikari et al. [27] considers the effects of bending and axial deformations of the cell walls. The current expressions can be further reduced to the classical formulas of Gibson and Ashby [19] (for the case of passive hexagonal lattices accounting only the bending deformation of the cell walls) by substituting the values of α, V and κ equals to zero (refer to the supplementary material for further details). In case of active lattices, considering the cell walls to be axially rigid, the obtained expressions reduce to the expressions obtained by Singh et al. [26]. The above discussion shows that the current formulation leading to the modulation of active Poisson's ratios and Young's moduli in a closed-form framework is analytically validated in an exact manner with published literature. The beam-level numerical validation along with exact analytical validation at the lattice level provide adequate confidence for exploring the aspect of active modulation and sign reversal of elastic properties in lattice materials based on the derived formulation. In the current investigation, T_{total}/L ($T_{total} = nT_p + T_s$, where n=1, 2 for unimorph and bimorph configuration respectively) has been kept to be $\sim 10^{-2}$ along with $\alpha = 0.5$ ($\alpha = \frac{T_p}{T_s}$) and $T_s = 0.68$ mm. TPU and M2814-P2 have been selected for substrate beam and piezoelectric material having Y_s and Y_p as 9.4 MPa and 30.3 Gpa, respectively [42].

The active modulation of Poisson's ratios are numerically demonstrated in Figs. 3 and 4 as a function of applied voltage, mechanical stress and the microstructural geometry. The figures reveal that there exists specific $\frac{V}{\sigma_1}$ and $\frac{V}{\sigma_2}$ values for every cell angle where the sign reversal of ν_{12} and ν_{21} can be observed depending on the piezoelectric configuration and actuation condition. The results indicate that it is possible to have negative Poisson's ratio in a geometrically non-auxetic lattice and vice-versa. The analytical conditions for such phenomenon can be obtained by substituting the numerator and the denominator of the respective closed-form expressions of the Poisson's ratios to less than equal to zero separately. There exists two conditions mentioned in Eq. (3) and (4) for which the reversal of ν_{12} would occur, as deduced from Eq. (1). Similarly, for ν_{21}, Eqs. (5) and (6) gives the conditions required for the sign reversal, as obtained from Eq. (2). From these pair of conditions mentioned here, only one should be satisfied at an instant to obtain the desired effect.

Condition 1 for the sign reversal of ν_{12} (for both unimorph and bimorph configurations):

$$\frac{V}{\sigma_1} > \frac{W_s L^2 \cos^2\theta\,(\beta + \sin\theta)\,\lambda_{P2}}{B_p L \lambda_{BP2}\frac{K_{55}}{K_{44}} - 6J_p \cos\theta \lambda_{JP2}} \tag{3}$$

Condition 2 for the sign reversal of ν_{12} (for both unimorph and bimorph configuration):

$$\frac{V}{\sigma_1} < \frac{-W_s L^2 \cos\theta\,(\beta + \sin\theta)\,\lambda_{P1}}{B_p L \lambda_{BP1}\frac{K_{55}}{K_{44}} + 6J_p \lambda_{JP1}} \tag{4}$$

Condition 1 for the sign reversal of ν_{21} (for both unimorph and bimorph configuration):

$$\frac{V}{\sigma_2} > \frac{W_s L^2 \cos^2\theta \lambda_{W1}}{B_p L \lambda_{BW1}\frac{K_{55}}{K_{44}} - 6J_p \lambda_{JW1}} \tag{5}$$

Condition 2 for the sign reversal of ν_{21} (for both unimorph and bimorph configuration):

$$\frac{V}{\sigma_2} < \frac{-W_s L^2 \cos^3\theta \lambda_{W2}}{B_p L \lambda_{BW2}\frac{K_{55}}{K_{44}} + 6J_p \cos\theta \lambda_{JW2}} \tag{6}$$

Note that, there could be only one actuation scenario for the unimorph configuration as shown in Fig. 2 (refer to the subsequent numerical results presented in Figs. 3(a) and 4(a)), while multiple cases are possible for the bimorph configurations. The unimorph configurations allow us to modulate the Poisson's ratios depending on voltage, along with the sign reversal of Poisson's ratios. Note that, for any elastic modulus, we say an active modulation/ sign reversal is possible, only when the colour of the plots can be changed along a vertical line for any value of the cell angle (the blue and red gradient in colour bar represent the positive and negative values of the corresponding elastic modulus). In the following paragraphs, we discuss the results further for the bimorph configuration considering different actuation scenarios as discussed in Fig. 1(j) and Fig. 2. The geometry of the bimorph structure is symmetric, consisting of one piezoelectric material at the top and the other at the bottom; this gives us the value of K_{64} equals to zero (as derived in the supplementary material). For bimorph configuration, cases have been divided into three categories mentioned below.

Case 1: Hybrid actuation. In this scenario, the top and the bottom piezoelectric material are under the influence of different voltages, i.e., V_t and V_b are different. The voltages can be of any polarity, and this condition will prevail until the magnitudes of the applied voltage are different. The other necessary parameters for analysing the Poisson's ratios under hybrid actuation can be obtained from Table 1. For obtaining the numerical results, $\frac{V_b}{\sigma_1}$ has been kept equal to −200,

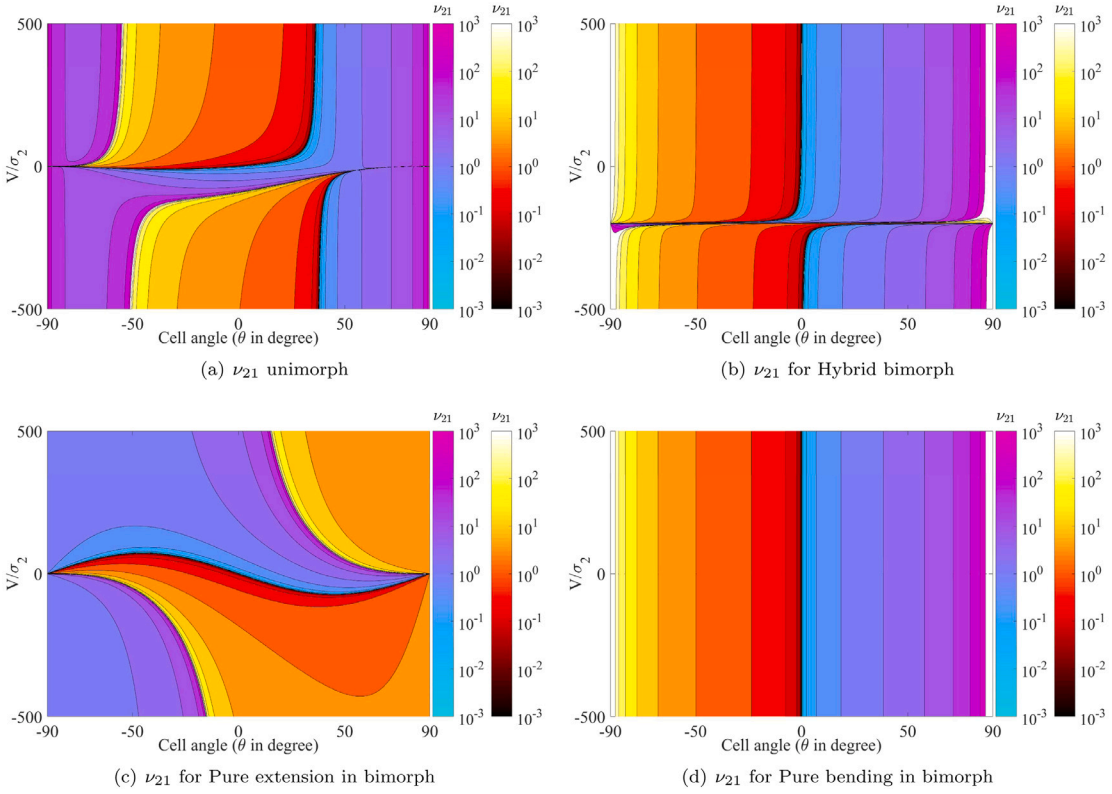

Fig. 4. Active modulation of ν_{21}. The Poisson's ratio ν_{21} has been plotted for all the different possible cases. (a) Unimorph configuration (b) Hybrid actuation in bimorph configuration (c) Pure extension in bimorph configuration (d) Pure bending in bimorph configuration. Variation in ν_{21} with cell angle and $\frac{V}{\sigma_1}$ (for hybrid bimorph $\frac{V_t}{\sigma_1}$ is varied and $\frac{V_b}{\sigma_1}$ has been kept equal to −200; V_t and V_b stand for the voltage applied to the top and bottom piezoelectric layer, respectively) ratio are analysed at a fixed value of $\beta = 2.5$. A clear reversal of sign for Poisson's ratio can be observed in the case of hybrid actuation (bimorph). Note that the blue and red gradient in colour bar represents the positive and negative values.

whereas $\frac{V_t}{\sigma_1}$ has been varied from −500 to 500. Along with prospective on-demand modulation, the sign reversal of the Poisson's ratios can be noted for a small range in Figs. 3(b) and 4(b).

Case 2: Pure extension. In this scenario, the voltage is applied in such a manner that the piezoelectric material contributes to axial displacement only as shown in Fig. 2(b), i.e., both the piezoelectric materials are under the influence of voltage having the same magnitude and polarity, i.e., $V_t = V_b$. Under the above mentioned conditions we get B_pV equals to $2W_pd_{31}Y_pV$ and J_pV equals to zero as shown in Table 1. Here, the switching of the Poisson's ratio is observed as shown in Figs. 3(c) and 4(c). Further, the voltage-dependent active modulation is also possible.

Case 3: Pure bending. In this scenario, the voltage is applied in such a manner that piezoelectric material contributes to pure bending (and no extension) as shown in Fig. 2(c), i.e., both the piezoelectric materials are under the influence of voltage having the same magnitude but opposite polarity, i.e., V_t=-V_b. Under the above mentioned conditions, we get B_pV equals to zero as shown in Table 1, whereas the value of J_pV is $W_pd_{31}Y_pT_s\,(1+\alpha)\,V$. In this case, the on-demand modulation and the switching of the Poisson's ratios are not possible as shown in Fig. 3(d) and Fig. 4(d).

2.2. Young's modulus

Even though the main focus of this paper is active Poisson's ratio modulation, we have investigated the Young's moduli of such lattices as an integral part of this investigation following the current analytical framework of accounting both the axial and bending deformations of the cell walls. In this section we will discuss the voltage dependency of longitudinal/transverse Young's modulus ($\bar{E}_1 = \frac{E_1}{Y_s} \times 10^7$ and $\bar{E}_2 = \frac{E_2}{Y_s} \times 10^7$) along with all the critical values at which the sign reversal of $\bar{E}_1$ and $\bar{E}_2$ takes place. The closed-form expressions for the effective Young's moduli can be given as Eqs. (7) and (8) (refer to the supplementary material for derivation). These general expressions are valid for both unimorph and bimorph configurations.

$$E_1 = \frac{K_{55}}{W_s\,(\beta + \sin\theta)\cos\theta\lambda_{P1} + \frac{B_pV\lambda_{BP1}}{\sigma_1 L}\frac{K_{55}}{K_{44}} + \frac{6J_pV\lambda_{JP1}}{\sigma_1 L^2}} \tag{7}$$

$$E_2 = \frac{K_{55}}{W_s\cos^3\theta\lambda_{W2} + \frac{B_pV\lambda_{BW2}}{\sigma_2 L}\frac{K_{55}}{K_{44}} + \frac{6J_pV\cos\theta\lambda_{JW2}}{\sigma_2 L^2}} \tag{8}$$

In Figs. 5(a), 5(b), 5(c) and 5(d), the variation in the Young's modulus ($\bar{E}_1$) with the cell angle and $\frac{V}{\sigma_1}$ ratio has been plotted for all the different cases (refer to Fig. 1(j)). Here, the blue gradient represents the positive Young's modulus, whereas the red gradient stands for the negative Young's modulus. For hybrid actuation, unequal voltage is applied to the top (V_t) and bottom (V_b) piezoelectric layers. The sign reversal phenomenon of Young's modulus ($\bar{E}_1$) is observed with the change in the cell angle and $\frac{V}{\sigma_1}$ ratio for all the four cases of unimorph and bimorph configurations. From Eq. (7) it can be observed that $\bar{E}_1$ would be negative when the value of the denominator is less than zero. The critical values of $\frac{V}{\sigma_1}$ at which $\bar{E}_1$ becomes negative, can be obtained from Eq. (9). It can be observed from (9) and 5(a), 5(b) and 5(d) that the sign of cell angle is playing a major role in determining the sign of $\bar{E}_1$. However, $\bar{E}_1$ for pure extension bimorph configuration comes out to be independent of the sign of cell angle for negative values of $\frac{V}{\sigma_1}$

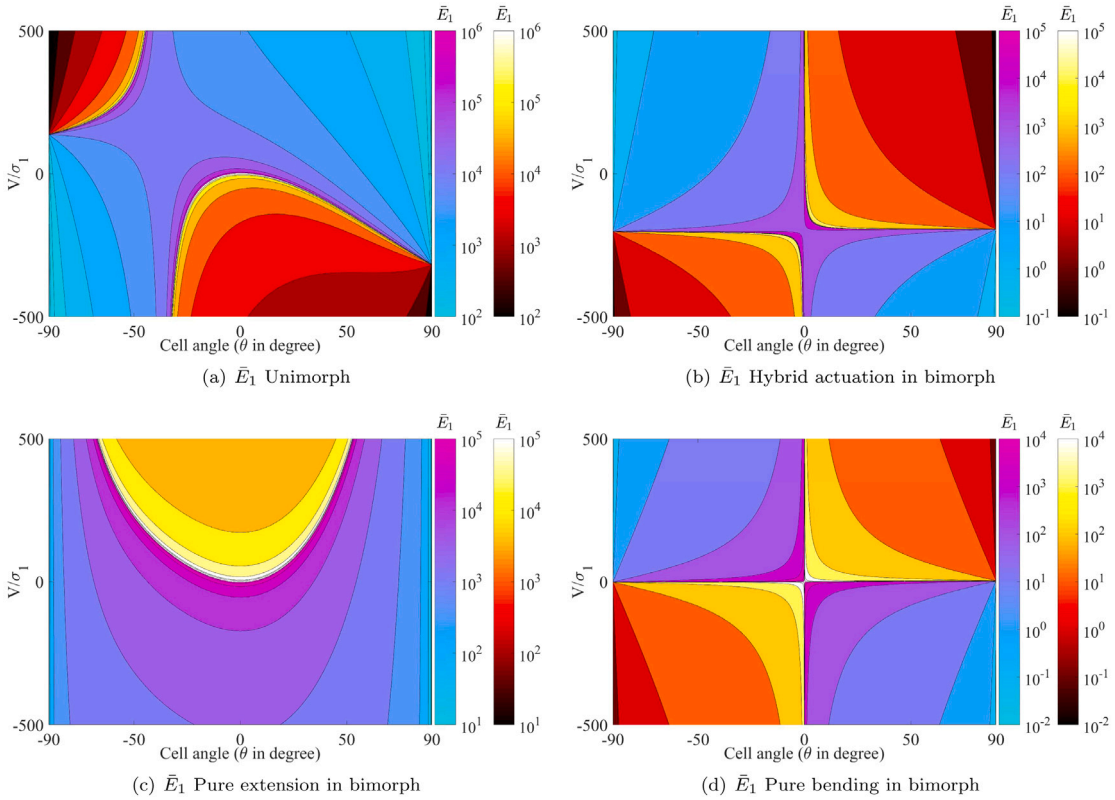

Fig. 5. Active modulation of $\bar{E}_1$. The Young's modulus $\bar{E}_1$ has been plotted for all the different possible cases. (a) Unimorph configuration (b) Hybrid actuation in bimorph configuration (c) Pure extension in bimorph configuration (d) Pure bending in bimorph configuration. Variation in $\bar{E}_1$ with cell angle and $\frac{V}{\sigma_1}$ (for hybrid bimorph $\frac{V_t}{\sigma_1}$ is varied and $\frac{V_b}{\sigma_1}$ has been kept equal to −200; V_t and V_b stand for the voltage applied to the top and bottom piezoelectric layer, respectively) ratio are analysed at a fixed value of $\beta = 2.5$. A clear reversal of sign for $\bar{E}_1$ can be observed in all the cases. Note that the blue and red gradient in colour bar represents the positive and negative values.

ratio.

$$\frac{V}{\sigma_1} < \frac{-W_s L^2 \cos\theta(\beta + \sin\theta)\lambda_{P1}}{B_p L \lambda_{BP1} \frac{K_{55}}{K_{44}} + 6 J_p \lambda_{JP1}} \tag{9}$$

Based on Eq. (8), the critical values of $\frac{V}{\sigma_2}$ at which the sign reversal of $\bar{E}_2$ occurs can be obtained as given in Eq. (10). Fig. 6 shows the variation in $\bar{E}_2$ with cell angle and $\frac{V}{\sigma_2}$ ratio, wherein both the aspects of active modulation and sign reversal can be observed for all the four cases.

$$\frac{V}{\sigma_2} < \frac{-W_s L^2 \cos^2\theta \lambda_{W2}}{B_p L \lambda_{BW2} \frac{K_{55}}{K_{44}} + 6 J_p \cos\theta \lambda_{JW2}} \tag{10}$$

2.3. Summary

The physics-based analytical framework for voltage-dependent on-demand Poisson's ratio modulation, as presented in this article, provides necessary physical insights and background for potential practical applications in various futuristic multi-functional structural systems and devices. The major outcomes and observations of the current investigation are summarized below.

- The current framework of piezoelectric lattices allows active on-demand modulation of Poisson's ratios and Young's moduli as a function of applied voltage and mechanical stress along with the coupled effect of conventional microstructural material and geometric parameters. Such active multi-physical modulation of the elastic properties are achievable for all the unimorph and bimorph configurations.
- For the bimorph configurations, sign reversal in both the in-plane Poisson's ratios can be achieved in the hybrid actuation and pure extension cases. For the unimorph configuration, ν_{12} and ν_{21} both shows such capability.
- The active sign reversal capability for the two Young's moduli can be achieved in all the four cases of unimorph and bimorph configurations.
- The theoretical conditions of sign reveal and active property modulations have been derived in closed-form for all the Poisson's ratios and Young's moduli.

3. Conclusions and perspective

This article proposes hybrid lattice microstructures comprised of a substrate and piezoelectric material to demonstrate the capability of active property modulation along with on-demand sign reversal. A bottom-up analytical framework has been adopted, based on which the closed-form expressions of the Poisson's ratios and Young's moduli along with the respective theoretical conditions for sign reversal have been derived. Usually, the elastic properties depend on the microstructural geometric and material properties, i.e. altering the elastic properties is impossible once the lattice is manufactured (passive lattices). This limits the application of such lattices in many advanced multi-functional structures and systems, where on-demand active property modulations are warranted. The current study proposes voltage-dependent closed-form expressions for the elastic properties of lattice materials; hence, active control is possible even after manufacturing the lattices. Here a general formulation has been presented that can be implemented for unimorph and bimorph configurations. Special cases in bimorph configuration such as pure bending, pure extension and hybrid actuation have been discussed in detail. Note that a beam-level numerical validation is provided first for the hybrid piezoelectric beams, followed by exact analytical validation and finite element based

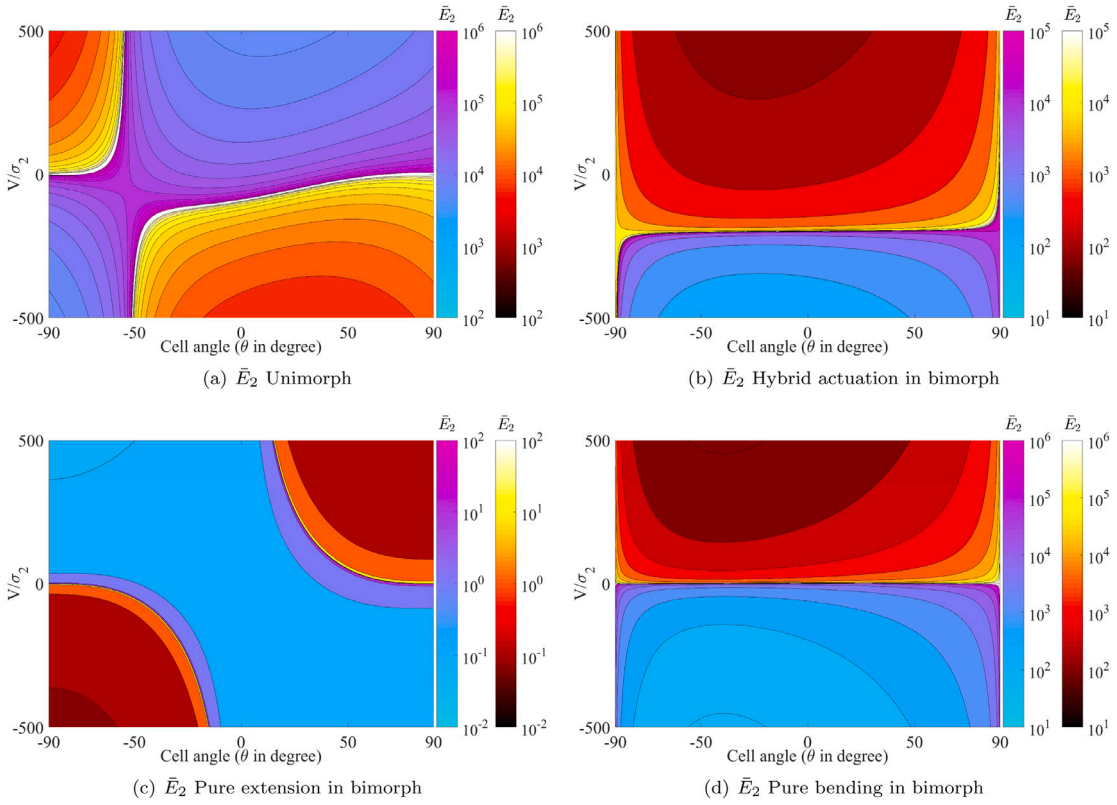

Fig. 6. Active modulation of $\bar{E}_2$. The Young's modulus $\bar{E}_2$ has been plotted for all the different possible cases. (a) Unimorph configuration (b) Hybrid actuation in bimorph configuration (c) Pure extension in bimorph configuration (d) Pure bending in bimorph configuration. Variation in $\bar{E}_2$ with cell angle and $\frac{V}{\sigma_1}$ (for hybrid bimorph $\frac{V_t}{\sigma_1}$ is varied and $\frac{V_b}{\sigma_1}$ has been kept equal to −200; V_t and V_b stand for the voltage applied to the top and bottom piezoelectric layer, respectively) ratio are analysed at a fixed value of $\beta = 2.5$. A clear reversal of sign for $\bar{E}_2$ can be observed in all the cases. Note that the blue and red gradient in colour bar represents the positive and negative values.

validation at the lattice-level to garner adequate confidence in the derived formulation. This article attempts for the first instance to derive voltage-dependent closed-form expressions including the effects of axial and bending deformation of the connecting beam-like elements, which resulted in achieving the active modulation capability of Poisson's ratios. Moreover, in a static condition, negative values for longitudinal and transverse Young's modulus have also been achieved. Note that, while the notion of negative Young's moduli is well-established in the dynamic regime, the published literature has scarce references of having negative Young's moduli in a static condition.

Lattice microstructures have gained considerable attention from the researchers over past few years in the field of novel functional material development. The modulation of Poisson's ratios and other elastic properties has been investigated primarily as a function of the microstructural configurations. The major contribution of the current work is developing active lattice microstructures, capable of on-demand property modulation including some of the extreme features such as sign reversal. Contrary to the conventional wisdom, such active sign reversal implies that re-entrant honeycomb lattices can exhibit positive Poisson's ratios and vice versa. In essence, this study gives a critical insight into bridging the auxetic and non-auxetic nature of honeycombs irrespective of their geometry. The proposed formulation is generic in nature and it can be immediately extended to the other derivatives of hexagonal shapes (such as rectangular and rhombic) along with different other lattice structures by considering appropriate unit cells. This investigation will open up a whole new field of applications across different length scales, concerning the active modulation and control of elastic moduli and shapes of multi-functional lattice microstructures.

Declaration of competing interest

The authors declare that they have no known competing financial interests or personal relationships that could have appeared to influence the work reported in this paper.

Acknowledgements

The authors acknowledge the financial support from Visvesvaraya PhD scheme, Media Lab Asia, Ministry of Electronics and Information Technology, Government of India, through a scholarship (Unique Awardee Number MEITY-PHD-888) and SPARC project (MHRD /ME /2018544). TM acknowledges the grant received from SERB, India (SRG/2020/001398). SA acknowledges the support of the UK-India Education and Research Initiative, United Kingdom through grant number UKIERI/P1212. The authors would also like to thank Prof. N. Tiwari (IIT Kanpur) for supporting the numerical validation using finite element software.

Appendix A. The values of parameter λ

The parameter (λ) used in the analytical formulation helps in making the proposed expressions more general. The value of (λ) is different for different configurations (unimorph and bimorph). The values of K_{44}, K_{64} and K_{55} have been mentioned in Table 1 for both unimorph and bimorph configurations. It is known that in bimorph configuration, the structure is symmetric, which makes K_{64} equals to zero (see the detailed derivation in supplementary material). There are six parameters for each type of loading, i.e., longitudinal (having suffix P) and transverse (having suffix W). B and J refers to the extensional and curvature component whereas, 1, 2 in the suffix stands for the strains in the

respective directions 1 and 2. The different parameters mentioned in the above formulation have been labelled as λ_{P1}, λ_{P2}, λ_{BP1}, λ_{BP2}, λ_{JP1}, λ_{JP2}, λ_{W1}, λ_{W2}, λ_{BW1}, λ_{BW2}, λ_{JW1} and λ_{JW2} and their closed-form expressions are given as

$$\lambda_{P1} = \frac{\tan^2\theta + \frac{K_{55}}{K_{44}} - \frac{6\tan\theta K_{64}}{LK_{44}} - \frac{12\tan^2\theta K_{64}^2}{L^2K_{44}K_{55}}}{1 - \frac{12K_{64}^2}{L^2K_{44}K_{55}}},$$

$$\lambda_{JP1} = \frac{\tan\theta - \frac{2K_{64}}{LK_{44}}}{1 - \frac{12K_{64}^2}{L^2K_{44}K_{55}}}, \lambda_{BP1} = \frac{1 - \frac{6K_{64}\tan\theta}{LK_{55}}}{1 - \frac{12K_{64}^2}{L^2K_{44}K_{55}}},$$

$$\lambda_{BP2} = \frac{\sin\theta + 6\cos\theta\frac{K_{64}}{LK_{55}}}{(\beta + \sin\theta)\left(1 - 12\frac{K_{64}^2}{L^2K_{44}K_{55}}\right)},$$

$$\lambda_{JP2} = \frac{1 + 2\frac{K_{64}}{LK_{44}}}{(\beta + \sin\theta)\left(1 - 12\frac{K_{64}^2}{L^2K_{44}K_{55}}\right)},$$

$$\lambda_{P2} = \frac{\tan\theta\left(1 - \frac{K_{55}}{K_{44}}\right) - 6\frac{K_{64}}{LK_{44}} - 12\tan\theta\frac{K_{64}^2}{L^2K_{44}K_{55}}}{(\beta + \sin\theta)\left(1 - 12\frac{K_{64}^2}{L^2K_{44}K_{55}}\right)},$$

$$\lambda_{BW1} = \frac{1 + 6\tan\theta\frac{K_{64}}{LK_{55}}}{\left(1 - 12\frac{K_{64}^2}{L^2K_{44}K_{55}}\right)},$$

$$\lambda_{W1} = \frac{\tan\theta\left(1 - \frac{K_{55}}{K_{44}}\right) + 6\frac{K_{64}}{LK_{44}} - 12\tan\theta\frac{K_{64}^2}{L^2K_{44}K_{55}} - 6\sec^2\theta\frac{K_{64}}{LK_{44}}}{\left(1 - 12\frac{K_{64}^2}{L^2K_{44}K_{55}}\right)},$$

$$\lambda_{JW1} = \frac{\tan\theta + 2\frac{K_{64}}{LK_{44}}}{\left(1 - 12\frac{K_{64}^2}{L^2K_{44}K_{55}}\right)},$$

$$\lambda_{W2} = \frac{1 + \tan^2\theta\frac{K_{55}}{K_{44}} + 2\sec^2\theta\frac{K_{55}}{K_{44}^h} - 6\tan\theta\frac{K_{64}}{LK_{44}} - 12\frac{K_{64}^2}{L^2K_{44}K_{55}} - 24\frac{K_{64}^2}{L^2K_{44}K_{44}^h}}{(\beta + \sin\theta)\left(1 - 12\frac{K_{64}^2}{L^2K_{44}K_{55}}\right)},$$

$$\lambda_{JW2} = \frac{1 - 2\tan\theta\frac{K_{64}}{LK_{44}}}{(\beta + \sin\theta)\left(1 - 12\frac{K_{64}^2}{L^2K_{44}K_{55}}\right)},$$

$$\lambda_{BW2} = \frac{\sin\theta - 6\cos\theta\frac{K_{64}}{LK_{55}}}{(\beta + \sin\theta)\left(1 - 12\frac{K_{64}^2}{L^2K_{44}K_{55}}\right)}$$

Appendix B. Supplementary data

Supplementary material related to this article can be found online at https://doi.org/10.1016/j.compstruct.2021.114857.

References

[1] Zhang Y, Qiu X, Fang D. Mechanical properties of two novel planar lattice structures. Int J Solids Struct 2008;45(13):3751–68.

[2] Mukhopadhyay T, Adhikari S, Batou A. Frequency domain homogenization for the viscoelastic properties of spatially correlated quasi-periodic lattices. Int J Mech Sci 2019;150:784–806.

[3] Shan S, Kang SH, Zhao Z, Fang L, Bertoldi K. Design of planar isotropic negative Poisson's ratio structures. Extrem Mech Lett 2015;4:96–102.

[4] Wei L, Zhao X, Yu Q, Zhu G. A novel star auxetic honeycomb with enhanced in-plane crushing strength. Thin-Walled Struct 2020;149:106623.

[5] Berger J, Wadley H, McMeeking R. Mechanical metamaterials at the theoretical limit of isotropic elastic stiffness. Nature 2017;543(7646):533–7.

[6] Mukhopadhyay T, Ma J, Feng H, Hou D, Gattas JM, Chen Y, et al. Programmable stiffness and shape modulation in origami materials: Emergence of a distant actuation feature. Appl Mater Today 2020;19:100537.

[7] Bückmann T, Thiel M, Kadic M, Schittny R, Wegener M. An elasto-mechanical unfeelability cloak made of pentamode metamaterials. Nature Commun 2014;5.

[8] Zhu R, Liu X, Hu G, Sun C, Huang G. Negative refraction of elastic waves at the deep-subwavelength scale in a single-phase metamaterial. Nature Commun 2014;5.

[9] Fleck NA, Deshpande VS, Ashby MF. Micro-architectured materials: past, present and future. Proc R Soc A 2010;2495–516.

[10] Mukhopadhyay T, Adhikari S, Alu A. Theoretical limits for negative elastic moduli in subacoustic lattice materials. Phys Rev B 2019;99:094108.

[11] Du Y, Keller T, Song C, Wu L, Xiong J. Origami-inspired carbon fiber-reinforced composite sandwich materials – fabrication and mechanical behavior. Compos Sci Technol 2021;205:108667.

[12] Mukhopadhyay T, Adhikari S. Effective in-plane elastic properties of auxetic honeycombs with spatial irregularity. Mech Mater 2016;95:204–22.

[13] Wang H, Zhao D, Jin Y, Wang M, Mukhopadhyay T, You Z. Modulation of multi-directional auxeticity in hybrid origami metamaterials. Appl Mater Today 2020;20:100715.

[14] Gaal V, Rodrigues V, Dantas SO, Galvão DS, Fonseca AF. New zero Poisson's ratio structures. Phys Status Solidi (RRL) – Rapid Res Lett 2020;14(3):1900564.

[15] Huang J, Zhang Q, Scarpa F, Liu Y, Leng J. Multi-stiffness topology optimization of zero Poisson's ratio cellular structures. Composites B 2018;140:35–43.

[16] Olympio KR, Gandhi F. Zero Poisson's ratio cellular honeycombs for flex skins undergoing one-dimensional morphing. J Intell Mater Syst Struct 2010;21(17):1737–53.

[17] Attard D, Grima JN. Modelling of hexagonal honeycombs exhibiting zero Poisson's ratio. Phys Status Solidi B 2011;248(1):52–9.

[18] Gong X, Huang J, Scarpa F, Liu Y, Leng J. Zero Poisson's ratio cellular structure for two-dimensional morphing applications. Compos Struct 2015;134:384–92.

[19] Gibson L, Ashby MF. Cellular solids structure and properties. Cambridge, UK: Cambridge University Press; 1999.

[20] Malek S, Gibson L. Effective elastic properties of periodic hexagonal honeycombs. Mech Mater 2015;91(1):226–40.

[21] Mukhopadhyay T, Mahata A, Adhikari S, Zaeem MA. Effective elastic properties of two dimensional multiplanar hexagonal nanostructures. 2D Mater 2017;4(2):025006.

[22] Abd El-Sayed F, Jones R, Burgess I. A theoretical approach to the deformation of honeycomb based composite materials. Composites 1979;10(4):209–14.

[23] Masters I, Evans K. Models for the elastic deformation of honeycombs. Compos Struct 1996;35(4):403–22.

[24] Zhang J, Ashby M. The out-of-plane properties of honeycombs. Int J Mech Sci 1992;34(6):475–89.

[25] Adhikari S, Mukhopadhyay T, Shaw A, Lavery N. Apparent negative values of Young's moduli of lattice materials under dynamic conditions. Internat J Engrg Sci 2020;150:103231.

[26] Singh A, Mukhopadhyay T, Adhikari S, Bhattacharya B. Voltage-dependent modulation of elastic moduli in lattice metamaterials: Emergence of a programmable state-transition capability. Int J Solids Struct 2021;208–209:31–48.

[27] Adhikari S, Mukhopadhyay T, Liu X. Broadband dynamic elastic moduli of honeycomb lattice materials: A generalized analytical approach. Mech Mater 2021;103796.

[28] Grima JN, Jackson R, Alderson A, Evans KE. Do zeolites have negative Poisson's ratios? Adv Mater 2000;12(24):1912–8.

[29] Song F, Zhou J, Xu X, Xu Y, Bai Y. Effect of a negative Poisson ratio in the tension of ceramics. Phys Rev Lett 2008;100(24).

[30] Lakes R. Foam structures with a negative Poisson's ratio. Science 1987;235(4792):1038–40.

[31] Schenk M, Guest SD. Geometry of miura-folded metamaterials. Proc Natl Acad Sci 2013;110(9):3276–81.

[32] Chetcuti E, Ellul B, Manicaro E, Brincat J-P, Attard D, Gatt R, et al. Modeling auxetic foams through semi-rigid rotating triangles. Phys Status Solidi B 2014;251(2):297–306.

[33] Bacigalupo A, Gambarotta L. Chiral two-dimensional periodic blocky materials with elastic interfaces: Auxetic and acoustic properties. Extrem Mech Lett 2020;39:100769.

[34] Xu N, Liu H-T, An M-R, Wang L. Novel 2D star-shaped honeycombs with enhanced effective Young's modulus and negative Poisson's ratio. Extrem Mech Lett 2021;43:101164.

[35] Li X, Wang Q, Yang Z, Lu Z. Novel auxetic structures with enhanced mechanical properties. Extrem Mech Lett 2019;27:59–65.
[36] Evans KE. Auxetic polymers: a new range of materials. Endeavour 1991;15(4):170–4.
[37] Harkati E, Daoudi N, Bezazi A, Haddad A, Scarpa F. In-plane elasticity of a multi re-entrant auxetic honeycomb. Compos Struct 2017;180:130–9.
[38] Srivastava R, Bhattacharya B. Thermoelastic and vibration response analysis of shape memory alloy reinforced active bimorph composites. Smart Mater Struct 2020;30(1).
[39] Dwivedi A, Banerjee A, Bhattacharya B. Simultaneous energy harvesting and vibration attenuation in piezo-embedded negative stiffness metamaterial. J Intell Mater Syst Struct 2020;31(8):1076–90.
[40] Crawley EF, Anderson EH. Detailed models of piezoceramic actuation of beams. J Intell Mater Syst Struct 1990;1(1):4–25.
[41] Crawley EF, de Luist J. Use of piezoelectric actuators as elements of intelligent structures. Am Inst Aeronaut Astronaut J 1987;25(10):1373–85.
[42] Zhang J, Tu J, Li Z, Gao K, Xie H. Modeling on actuation behavior of macro-fiber composite laminated structures based on sinusoidal shear deformation theory. Appl Sci 2019;9(14).